MEDICAL SCIENCE MONITOR

CLINICAL RESEARCH

e-ISSN 1643-3750
© Med Sci Monit, 2019; 25: 2802-2810
DOI: 10.12659/MSM.915916

Received: 2019.02.26
Accepted: 2019.03.28
Published: 2019.04.16

3D Computed Tomography Mapping of Thoracolumbar Vertebrae Fractures

Authors' Contribution:
Study Design A
Data Collection B
Statistical Analysis C
Data Interpretation D
Manuscript Preparation E
Literature Search F
Funds Collection G

ACE 1 Qihang Su*
BE 1 Yan Zhang*
BD 2 Shenghui Liao
C 1 Meijun Yan
D 1 Kai Zhu
F 1 Shuaifeng Yan
AE 3 Cong Li
AEG 1 Jun Tan

1 Department of Orthopedics, Shanghai East Hospital, Tongji University School of Medicine, Shanghai, P.R. China
2 School of Information Science and Engineering, Central South University, Changsha, Hunan, P.R. China
3 Department of Trauma Surgery, Shanghai East Hospital, Tongji University School of Medicine, Shanghai, P.R. China

* Qihang Su and Yan Zhang contributed equally to this work and share first authorship

Corresponding Authors: Jun Tan: e-mail: dr_tanjun@tongji.edu.cn, Cong Li, e-mail: 15900549514@163.com
Source of support: The study was funded by the Programs for Academic Leaders in Shanghai Pudong New Area (PWRd-2011-02, PWRI2012-03)

Background: Fractures of the thoracolumbar (TL) spine represent 90% of all spinal fractures, followed by cervical and lumbar spine fractures. This study aimed to create fracture maps of the traumatic thoracolumbar (TL) fracture vertebral body (T12-L2) through the use of CT mapping as a big data visualization method to reveal recurrent patterns and characteristics of traumatic TL fractures.

Material/Methods: A consecutive series of 174 fractured vertebrae (T12–L2) was used to create three-dimensional (3D) reconstruction images, which were superimposed and oriented to fit a model vertebral template by aligning specific bio-landmarks and reducing reconstructed fracture fragments. Fracture lines were found and traced to create a fracture map of the vertebral body.

Results: Our study consisted of 165 patients with an average age of 47 years. A total of 174 fractured vertebrae were collected, consisting of 59 T12 vertebral fractures, 60 L1 vertebral fractures, and 55 L2 vertebral fractures. Two-dimensional (2D) maps, 3D maps, and heat maps showed that the fracture lines tended to be concentrated in the upper third and anterior third of the vertebral body, as well as being distributed in annular wedges along the anterior and lateral sides of the vertebral body. When compared with T12, the distribution of fracture lines in L1 and especially in L2 was more scattered and disorganized.

Conclusions: Fracture maps revealed recurrent patterns and characteristics of the traumatic TL fracture vertebral body, which improves understanding of TL fractures, as well as helping to increase opportunities for follow-up research and aid clinical decision-making.

MeSH Keywords: Imaging, Three-Dimensional • Maps • Spinal Fractures • Tomography Scanners, X-Ray Computed

Full-text PDF: https://www.medscimonit.com/abstract/index/idArt/915916

Indexed in: [Current Contents/Clinical Medicine] [SCI Expanded] [ISI Alerting System] [ISI Journals Master List] [Index Medicus/MEDLINE] [EMBASE/Excerpta Medica] [Chemical Abstracts/CAS]

Background

Fractures of the thoracolumbar (TL) spine represent 90% of all spinal fractures, followed by cervical and lumbar spine fractures [1]. Damage to the thoracolumbar spine are frequently a result of high-energy injuries, resulting in potentially devastating consequences [2–4]. In a study of 1445 cases by Magerl and colleagues [5], the levels of main injury were T12, L1, and L2. Type A fractures were found in 66.1% of those cases. Therefore, the present study focused on Type A fractures of T12–L2.

Clinical assessment of patients with TL fractures can be challenging; therefore, diagnostic imaging methods such as the spine computed tomography (CT) often play an essential role in exact diagnosis and appropriate management [6,7]. With increasing concern over big data analytics, the distribution map of fracture lines (fracture mapping) based on 3D CT has also been widely used in orthopedic fields, including scapular fractures and tibial plateau fractures, to characterize fractures [8,9], which was initially described by Cole et al. [10,11]. However, it has rarely been used in the study of spinal fractures such as thoracolumbar fractures.

This study aimed to determine the location and frequency of fracture lines of a series of traumatic TL fracture vertebral bodies (T12–L2), and to produce fracture maps by means of 2D and 3D CT mapping techniques. We hypothesized that mapping fractures of the TL vertebral body would reveal recurrent patterns of fragments, fracture lines, and TL spine fracture characteristics, which could improve surgeons' recognition and understanding of TL spine fractures during diagnosis, preoperative planning, execution of spinal surgeries, and proper internal fixation. Additionally, we achieved big data visualization of fractures of the TL vertebral body, which could play a key role in further research on the biomechanics and morphology of thoracolumbar spine fractures.

Material and Methods

Patient cohort

We undertook a retrospective analysis of the CT imaging data of patients with a diagnosis of TL fractures in our department between February 2015 and August 2018, which was searched in the Picture Archiving and Communication System (PACS) database. Inclusion criteria were: (1) Patients must be 18 years or older, and less than 65 years; (2) They must have fractures involving Type A fractures of the T12-L2 vertebral body (Type A1.3 and Type A1.1 excluded, as per Magerl et al's AO fracture classification system) [5]; (3) They must have non-pathological and non-osteoporotic vertebral fractures; (4) Patients must have a short traumatic history (<1 week); and (5) There must be good-quality CT images available. Exclusion criteria were: (1) Patients who had fracture lines or anatomical landmarks obscured by foreign bodies; and (2) Patients with severe comminuted fractures or merely depressed or impacted fractures, in which it is difficult to determine fracture line conditions.

A total of 174 fractured vertebrae in 165 patients were included after evaluation by an experienced spine physician and the senior author using the original 3D CT rendering in the PACS. The Shanghai East Hospital (East Hospital Affiliated to Tongji University) Medical Ethics Committee approved the study protocol (16 August 2018), which complied with the relevant guidelines and regulations of the Shanghai Medical Ethics Committee. All included volunteers signed an informed consent form.

Fracture mapping

Digital Imaging and Communications in Medicine (DICOM) format raw data were acquired using a 64-channel CT scanner (Siemens Somatom Sensation, Siemens, Erlangen, Germany) with the following parameters (Tube voltage, 120 kV; Tube current, 200 mA; Slice thickness, 1 mm; Interlayer spacing, 0.5 mm), and then imported into Mimics software (V20.0, Materialise, Inc., Leuven, Belgium) to create a project file. Fractures were analyzed simultaneously in the axial, sagittal, and coronal planes, allowing us to generate a 3D reconstruction of the fractured vertebral body.

The fractured vertebral body of T12–L2 was our region of interest (ROI) (Figure 1A). According to anatomical characteristics, we were able to establish 2 sagittal planes on the medial side of the pedicle, 2 coronal planes that divided the superior endplate of the vertebral body into 3 equal parts, and 2 axial planes from the middle, between the lower margin of the pedicle and the upper and lower edge of the pedicle (Figure 1B). The vertebral body was divided into 27 cubes by this 3-3-3 scheme. The upper 9 cubes were named Upper-Left-1~3 (UL-1~3), Upper-Middle-1~3 (UM-1~3), and Upper-Right-1~3 (UR-1~3). The middle 9 cubes were named Middle-Left-1~3 (ML-1~3), Middle-Middle-1~3 (MM-1~3) and Middle-Right-1~3 (MR-1~3). Finally, the lower 9 cubes were named Lower-Left-1~3 (LL-1~3), Lower-Middle-1~3 (LM-1~3) and Lower-Right-1~3 (LR-1~3) (Figure 1C). This regionalization of the vertebral body via the 3-3-3 scheme can aid the study of the distribution of fracture lines from a 3D perspective.

Following the method of 2D fracture mapping described by Cole et al. [10] and Armitage et al. [8], 2D fracture mapping of T12–L2 was carried out for each of the 6 planes described above. Firstly, 6 views of the reformatted axial, sagittal, and coronal planes of all fractures were imported into Adobe Photoshop to overlap and orient fracture patterns onto a standard template image (Figure 2A). Proper alignment and normalization of fracture

Indexed in: [Current Contents/Clinical Medicine] [SCI Expanded] [ISI Alerting System] [ISI Journals Master List] [Index Medicus/MEDLINE] [EMBASE/Excerpta Medica] [Chemical Abstracts/CAS]

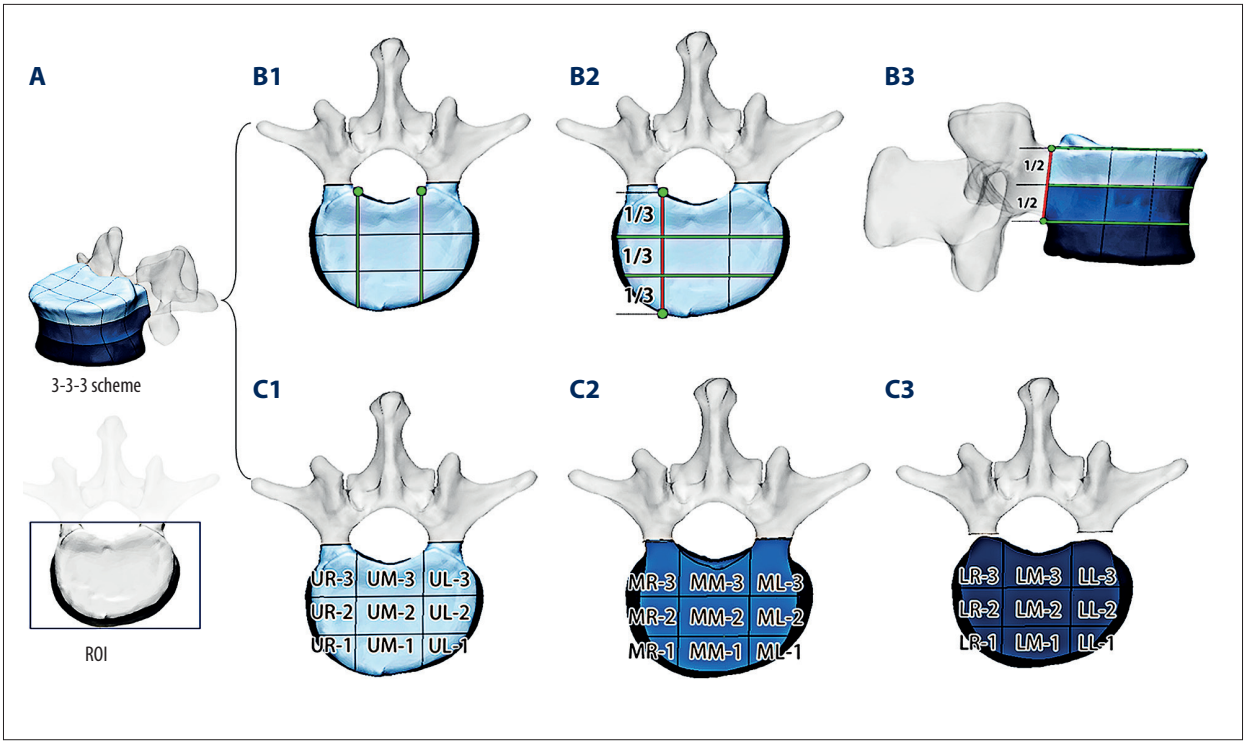

Figure 1. The regionalization of the vertebral body by the 3-3-3 scheme (**A**). The region of interest (ROI) of this study (**B1**). The establishment of 2 sagittal planes, 2 coronal planes (**B2**) and 2 axial planes (**B3**); the name of the upper 9 cubes (**C1**), middle 9 cubes (**C2**), and lower 9 cubes (**C3**).

fragments was undertaken by aligning specific vertebrae biolandmarks. Six planes of 2-D fracture mapping for each vertebral body were then obtained based on the overlap of fracture lines.

Following this, the 3D fracture map of the vertebral body (T12–L2) was drawn, using the method described by Xie et al. [12]. Firstly, vertebral fracture fragments were reconstructed in Mimics software and virtually reduced in order to create a 3D frequency diagram. Data were then exported into 3-matic software (V9.0, Materialise, Inc., Leuven, Belgium), in which reconstructed fragments were rotated, normalized, and horizontally flipped to optimally match the 3D model of the template vertebral body. Smooth curves were then drawn directly onto the surface of the model to delineate the fracture lines of each case (Figure 2B). A 3D fracture map of the vertebral body (T12–L2) was then obtained by analyzing the overlap of all the fracture lines.

Finally, heat maps of each vertebral body were acquired based on the 3D fracture maps in E-3D software (Central South University, Changsha, China).

Data analysis

Patient characteristics were summarized using frequencies and percentages for categorical variables and with arithmetic means for continuous variables [11]. To analyze the fracture maps, a 3D map of each cube was first obtained. The fracture line passing rate of each cube was then counted. Finally, using a combination of the 2D, 3D, and heat maps of each vertebral body, as well as the fracture line passing rate of each cube, descriptive analysis was completed.

Results

This study included data from 165 patients with 174 fractured vertebrae. There were 104 males and 61 females, with average age of 47 years and standard deviation (SD) of 9.54 years (Figure 3A). Patient demographics are summarized in Table 1.

The 174 fractured vertebrae were classified following Magerl et al. AO fracture classification system [5]. Distribution of fractures is summarized in Table 2, showing that most were Type A1 or Type A3. Among all the subtypes, it was found that Type A1.2.1 and Type A3.1.1 were predominant.

In addition, injury of the 174 fractured vertebrae was scored using McCormack et al. load-sharing classification (LSC) (Figure 3B) [13]. For the vertebral body T12, comminution/involvement (49/59; 83.05%), apposition/displacement of fracture fragments (48/59; 81.36%), and correction of kyphotic

Indexed in: [Current Contents/Clinical Medicine] [SCI Expanded] [ISI Alerting System] [ISI Journals Master List] [Index Medicus/MEDLINE] [EMBASE/Excerpta Medica] [Chemical Abstracts/CAS]

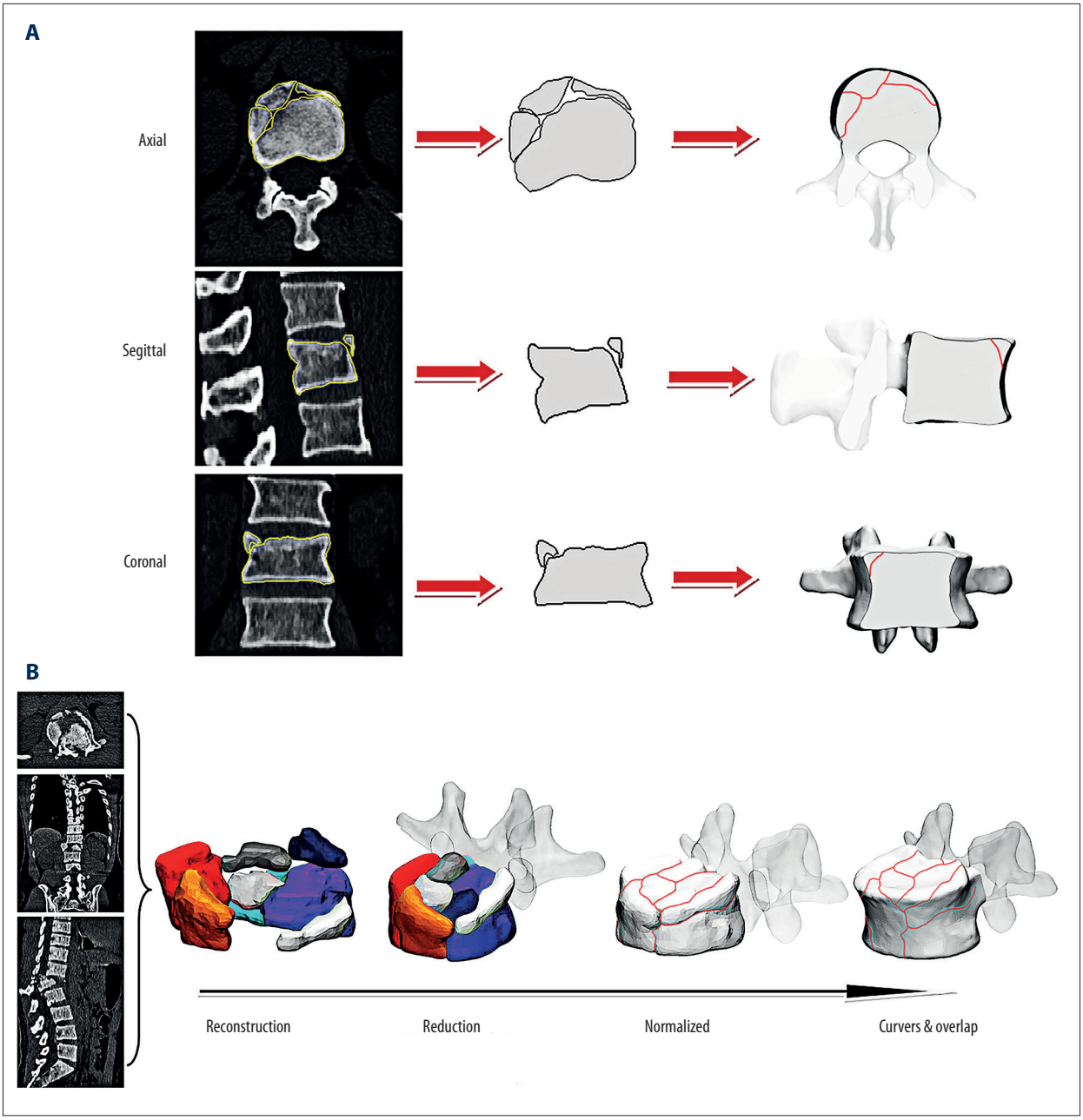

Figure 2. The process of 2D fracture mapping on the axial, sagittal, and coronal planes created. (**A**) The procedure of 3D fracture mapping. (**B**) The vertebral fracture fragments were reconstructed, reduced, and normalized to optimally match the standard template. Smooth curves were drawn directly on the surface of the model and then overlapped.

deformity (51/59; 86.44%) were mostly rated as 1. For vertebral bodies L1 and L2, the above 3 items were mostly scored 2 or 3.

Plane maps

Figure 4A shows 2D fracture maps of 6 planes in each segment of T12, L1, and L2. The 6 planes revealed that the fracture lines were mainly circularly distributed along the upper part and the anterior third of the vertebral body.

3D maps

Figure 4B shows the 3-D maps of T12, L1, and L2, which demonstrate the distribution of fracture lines in the 3 segments. One common feature of these 3D maps is that the fracture lines tend to be concentrated in the upper third and anterior third of the vertebra, as well as being arranged in annular wedges along the front and side of the vertebral body. This means that, as in the features of 2D maps, fracture lines are concentrated in these regions.

Indexed in: [Current Contents/Clinical Medicine] [SCI Expanded] [ISI Alerting System] [ISI Journals Master List] [Index Medicus/MEDLINE] [EMBASE/Excerpta Medica] [Chemical Abstracts/CAS]

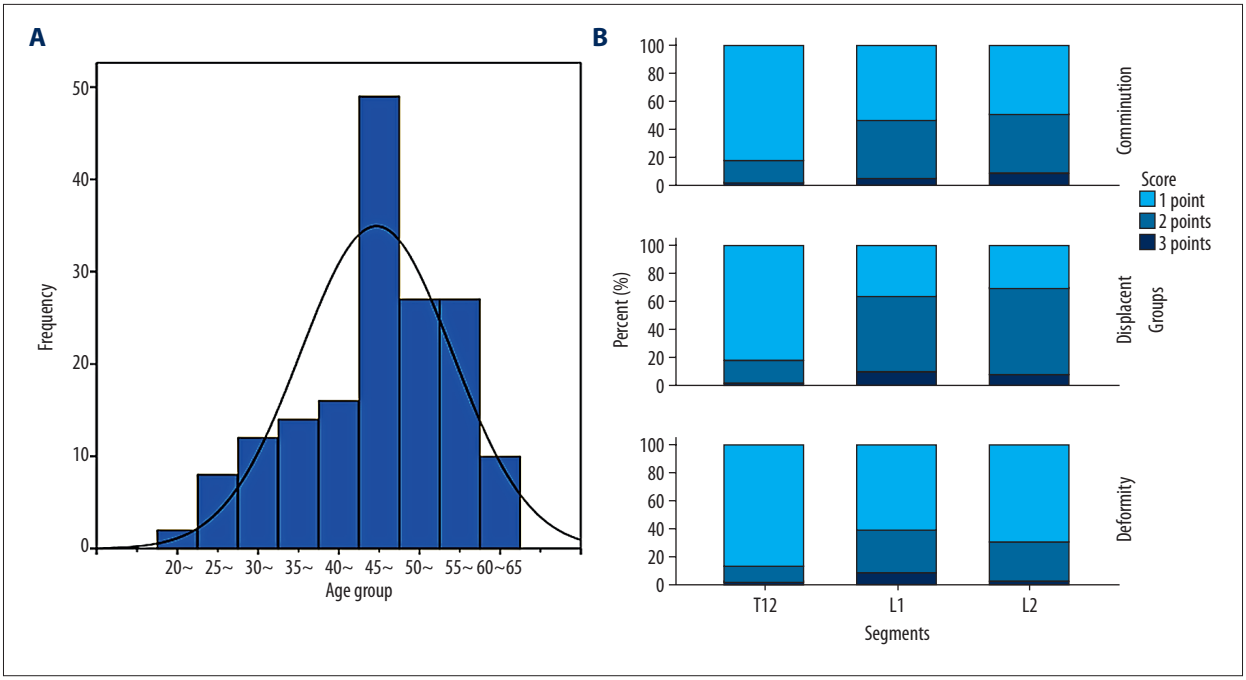

Figure 3. Histogram of age groups of all cases. (**A**) Percentage distribution diagram for the McCormack et al's LSC scoring of 174 fracture vertebrae. (**B**) Amount of comminution/involvement, the amount of apposition/displacement of fracture fragments, and the amount of correction of kyphotic deformity.

Table 1. Patient demographics (N=165).

Variables		
Gender (no.)		
Male (%)	104	(37.00)
Female (%)	61	(63.00)
Mean age [SD] (yr)	47	[9.54]
Total segments of fractures (no.)	174	
T12 (%)	59	(33.90)
L1 (%)	60	(34.50)
L2 (%)	55	(31.60)
Mechanism of injury (no.)		
Fall (%)	113	(68.48)
Traffic accident (%)	52	(31.52)

Additionally, the distribution of fracture lines of T12 was more concentrated and orderly. The fracture lines of L1 and especially L2 are more scattered and disorganized than those of T12, many of which run through the first 2 columns of the vertebrae, as defined by Dennis's concept of the 3-column spine [14,15].

The fracture line passing rate of each cube was calculated according to the 2D and 3D maps of each vertebral body (Figure 5A). There were 116 fracture lines in the T12 vertebral body. These fracture lines passed through its 27 cubes 390 times. There were 112 fracture lines for vertebral body L1, which passed through its 27 cubes 594 times. Vertebral body L2 had 135 fracture lines which passed through its 27 cubes 589 times. Similarly, the fracture line passing rate of the upper 9 cubes was higher than that of the middle group and the lower group. UM-1, UR-1, and UL-1 had higher fracture line passing rates than other cubes. In contrast to T12, both L1 or L2 had fracture line pass rates of UL-2 and UR-2, which were higher than that of UM-2.

Heat maps

The heat maps directly show density or frequency of spatial data relating to thoracolumbar fractures, similar to 3D maps. The main high incidence area of T12-L2 is located in UR-2, UR-1, UM-1, UL-1, and UL-2 (the red area), with a circular distribution (Figure 5B).

Discussion

Fracture mapping techniques were applied in a first attempt at analysis of thoracolumbar fractures. Using big data visualization techniques, 174 fracture vertebral bodies of T12–L2 were analyzed from the perspectives of epidemiology and morphology.

Indexed in: [Current Contents/Clinical Medicine] [SCI Expanded] [ISI Alerting System] [ISI Journals Master List] [Index Medicus/MEDLINE] [EMBASE/Excerpta Medica] [Chemical Abstracts/CAS]

Table 2. Fracture distribution (N=174).

Groups (Type A.)	T12	L1	L2	Total
A1. Impaction fractures (%)	34 (19.54)	30 (17.24)	38 (21.84)	102 (58.62)
A1.2.1	29	23	36	88
A1.2.2	3	4	2	9
A1.2.3	2	3	0	5
A2. Split fractures (%)	1 (0.57)	2 (1.15)	2 (1.15)	5 (2.87)
A2.1	1	1	0	2
A2.2	0	1	2	3
A2.3	0	0	0	0
A3. Burst fractures (%)	24 (13.79)	28 (16.09)	15 (8.62)	67 (38.51)
A3.1.1	12	17	10	39
A3.1.2	3	1	1	5
A3.1.3	1	1	0	2
A3.2.1	5	4	1	10
A3.2.2	1	1	1	3
A3.2.3	0	1	0	1
A3.3.1	0	2	0	2
A3.3.2	2	1	0	3
A3.3.3	0	0	2	2

While 3D mapping is both time-consuming and technically demanding, it is more accurate for the demonstration of fracture morphology than 2D mapping, and provides additional information that is crucial for preoperative planning and execution of surgical strategies [12,16]. Combining the results of this study with observations of the 2D, 3D, and heat maps of the vertebral body T12–L2 shows that the distribution of fracture lines in T12–L2 tends to be concentrated in the upper third and anterior third of the vertebral body, while distribution is circular along the upper edge of the vertebral body. The incidence rates of fractures vary greatly from UX-1~2, to MX-1~2, to LX-1~2 (X='L', 'M' or 'R'), and all are located in the anterior column of vertebrae. This means that UR-1~2, UM-1, and UL-1~2 can be seen as high incidence areas for fractures. Therefore, we speculated that these elements are the main force area or are relatively vulnerable during vertebral fracture, which provides a possibility to better understand and improve the 3-column concept and TL injury classification systems in biomechanics and morphology.

We found that the fracture line passing rates of UR-2, UM-2, and UL-2 in T12 are similar, while the 2D, 3D, and heat maps suggested that the density of fracture line distribution between UR-2 and UL-2 was larger than that of UM-2. This might due to the different volumes of the 3 cubes. Since we based the 3-3-3 frame on the anatomical characteristics of the vertebrae, the volume of UM-2 was greater than that of UR-2 and UL-2, which explains our mismatching of the fracture line passing rate and fracture line density. In this case, it seems reasonable to reflect the distribution of fracture lines by the density of fracture lines. Thus, mapping can provide clearer, more accurate information as well as enhancing our understanding.

To formulate an appropriate management strategy, accurate classification of the fracture is critical [7], but no TL injury classification system has achieved universal international acceptance [17]. Table 2 shows that the proportion of fracture Types of T12, L1, and L2 were similar, and that the total number of fracture lines of vertebral body L1 or L2 was similar to that of T12, while the total fracture line passing frequency of L1 and L2 was much higher than that of T12. The classification is primarily based on pathomorphological uniformity [5]. Combined with the LSC score (Figure 3B), we concluded that vertebral bodies L1 and L2, when compared with T12, are more seriously comminuted in morphology. Although neither of the classification systems is capable of thoroughly assessing TL fractures, the fracture maps can directly reveal recurrent patterns and characteristics of TL fractures shown by the combination of the 2 classification systems. Additionally, the 3D maps also revealed that the distribution of fracture lines in L1 and L2 was more dispersed, with larger spans.

Indexed in: [Current Contents/Clinical Medicine] [SCI Expanded] [ISI Alerting System] [ISI Journals Master List] [Index Medicus/MEDLINE] [EMBASE/Excerpta Medica] [Chemical Abstracts/CAS]

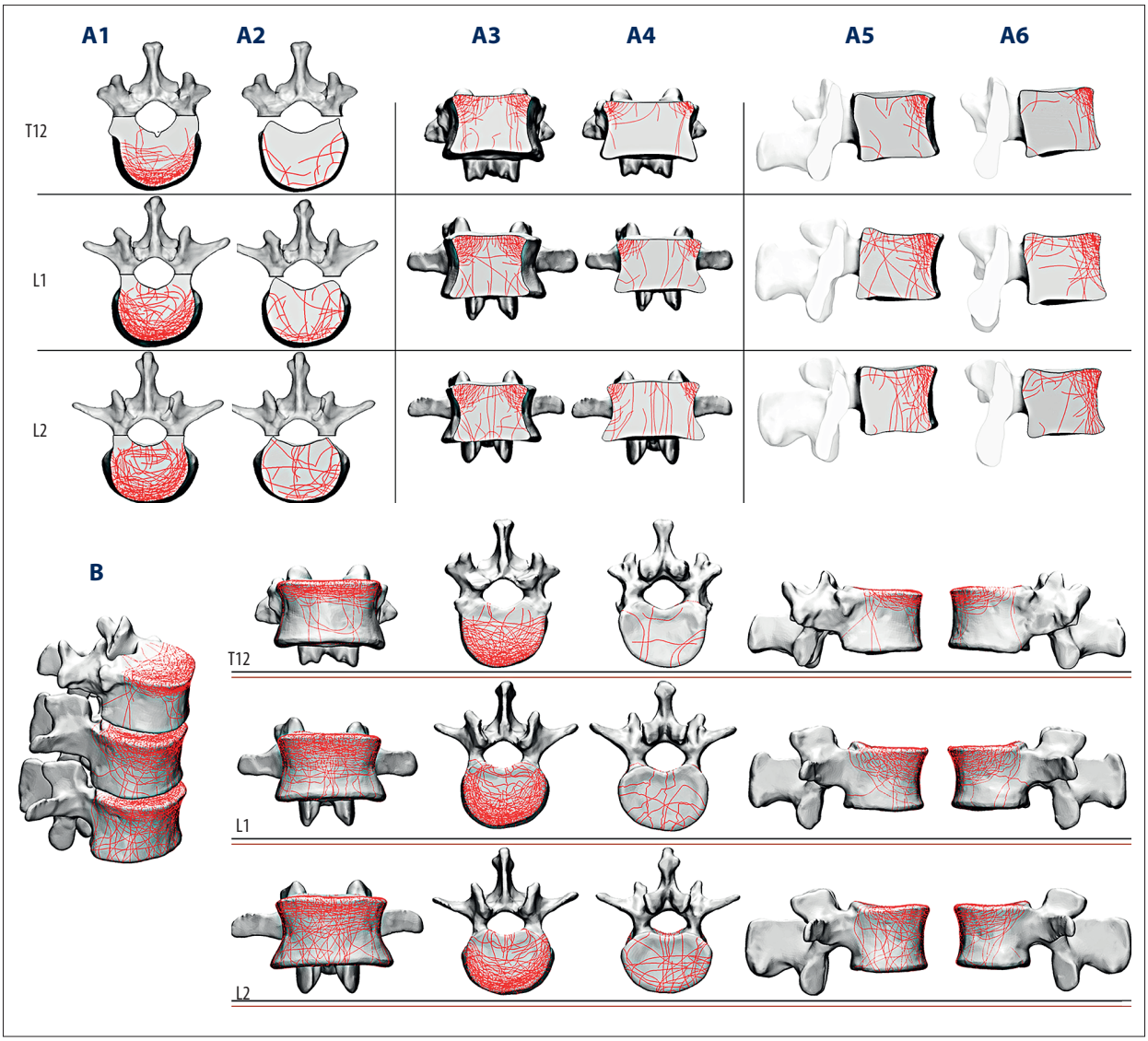

Figure 4. The 2D fracture maps of 6 planes in each segment of T12, L1, and L2. (**A**) The 2 axial planes from the middle, between the lower margin of the pedicle, and the upper (**A1**) and lower edge of the pedicle (**A2**); 2 coronal planes that divided the superior endplate of the vertebral body into 3 equal parts (**A3:** the anterior, **A4:** the posterior); 2 sagittal planes on the medial side of the pedicle (**A5:** the right, **A6:** the left). 3D maps of T12, L1, and L2. (**B**) Front view, top view, bottom view, right view, and left view (from left to right).

These characteristics may be related to the location of the vertebral bodies. The thoracolumbar region (T10–L2) is either straight or somewhat kyphotic (0°–10°) in the sagittal plane. The kyphotic position of the thoracic spine as well as the center of gravity of the body, located anterior to the spine, causes compressive forces to be transmitted above the vertebral body, along with a tensile stretch or distraction of the posterior sections. In the lordotic region of the lower lumbar spine, forces are transferred in a posterior position relative to the spine, meaning these compressive loads pass through the posterior elements [18,19]. This may be a reason why the fracture line distributions of L1 and L2 differ from that of T12. Therefore, the design of fracture internal fixation devices of T12 should be more focused than that of L1 and L2 on fixation of the upper third and anterior third of the vertebral body.

Our study has some limitations. Firstly, the ROI was vertebral body T12–L2, meaning other vertebral bodies were not included, nor were the related structures of the thoracolumbar posterior column. As an example, the ligaments behind the thoracolumbar spine are crucial for spinal stability and preoperative planning [20–22], meaning it is not possible to comprehensively evaluate the condition of a patient from just 2-D and 3-D fracture maps. Secondly, the study mainly analyzed

Indexed in: [Current Contents/Clinical Medicine] [SCI Expanded] [ISI Alerting System] [ISI Journals Master List] [Index Medicus/MEDLINE] [EMBASE/Excerpta Medica] [Chemical Abstracts/CAS]

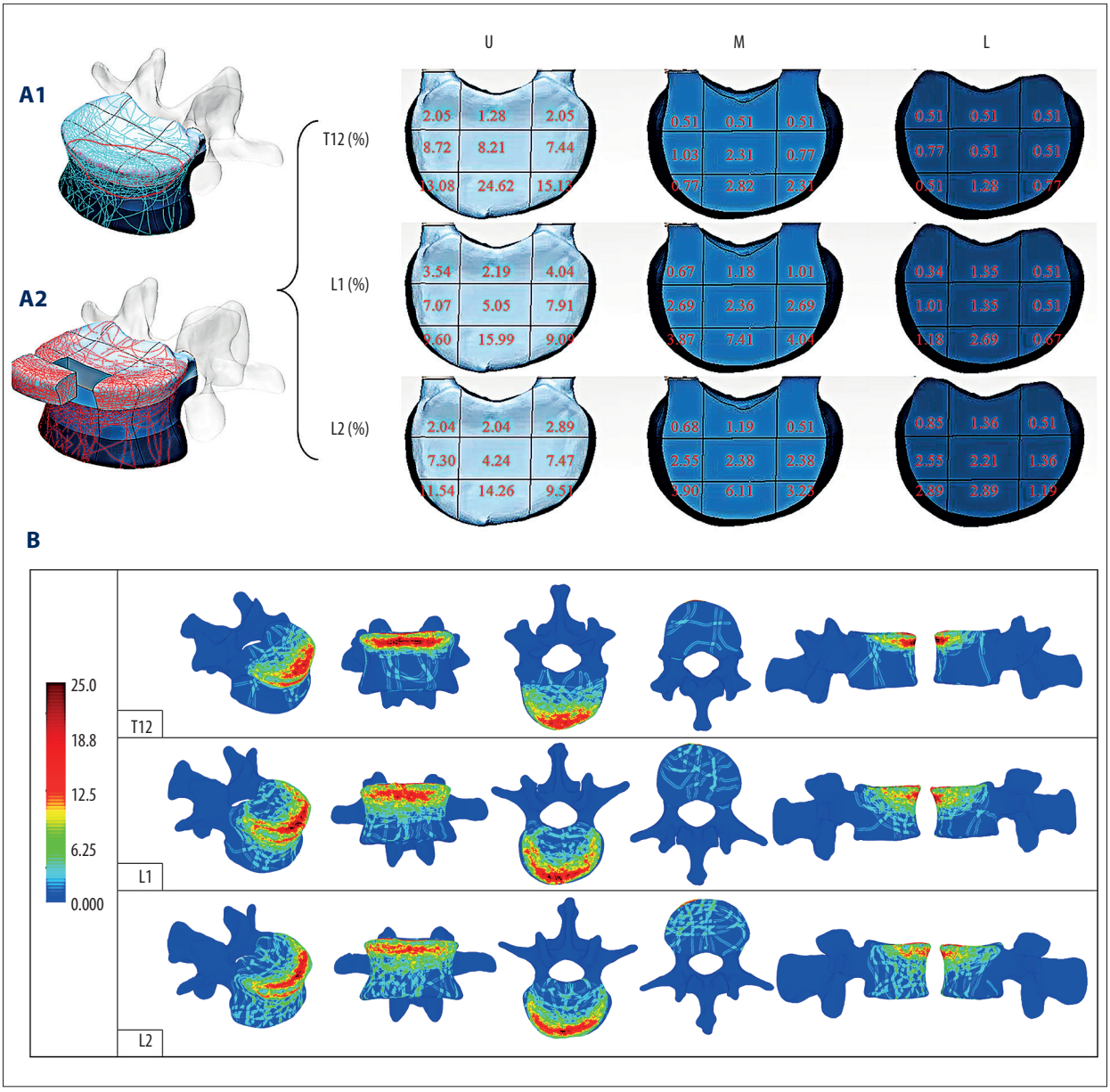

Figure 5. (**A**) The distribution of fracture line passing rate (%) for 27 cubes of each segment (T12, L1, L2): the fracture line passing rate (%)=the frequency of each cube/the total frequency of each vertebral body. (**A1, A2**) Upper 9 cubes (**U**), middle 9 cubes (**M**), and lower 9 cubes (**L**). (**B**) Heat maps of T12, L1, and L2: the isometric view, the front view, the top view, the bottom view, the right view, and the left view (from left to right).

fractures through morphology, while no detailed study of the thoracolumbar spine biomechanics was conducted. The vertebral body was divided into 27 cubes using a 3-3-3 scheme framework; this regionalization of the vertebral body has the potential to help researchers analyze local fractures, but it is much less detailed than finite element analysis (FEA) [23]. Therefore, further studies on thoracolumbar vertebra fracture with FEA will improve our understanding of thoracolumbar fractures.

Conclusions

Fracture maps revealed recurrent patterns and characteristics of traumatic TL fractured vertebral bodies (T12–L2), which provides us with a new understanding of thoracolumbar fractures from the perspectives of morphology and epidemiology, and enables us to further optimize surgical plans and design fracture internal fixation devices. In addition, these data may be useful for assessing the validity of existing fracture classification systems.

Indexed in: [Current Contents/Clinical Medicine] [SCI Expanded] [ISI Alerting System] [ISI Journals Master List] [Index Medicus/MEDLINE] [EMBASE/Excerpta Medica] [Chemical Abstracts/CAS]

Conflicts of Interest

None.

References:

1. Cahueque M, Cobar A, Zuniga C et al: Management of burst fractures in the thoracolumbar spine. J. Orthop, 2016; 13(4): 278–81
2. Wood KB, Li W, Lebl DS et al: Management of thoracolumbar spine fractures. Spine J, 2014; 14(1): 145–64
3. Fu MC, Nemani VM, Albert TJ: Operative treatment of thoracolumbar burst fractures: Is fusion necessary? HSS J, 2015; 11(2): 187–89
4. Zhang C, Liu Y: Combined pedicle screw fixation at the fracture vertebrae versus conventional method for thoracolumbar fractures: A meta-analysis. Int J Surg, 2018; 53: 38–47
5. Magerl F, Aebi M, Gertzbein SD et al: A comprehensive classification of thoracic and lumbar injuries. Eur Spine J, 1994; 3(4): 184–201
6. Anderson MW: Imaging of thoracic and lumbar spine fractures. Semin Spine Surg, 2010; 22(1): 8–19
7. Santiago FR, Muñoz PT, Sánchez EM et al: Classifying thoracolumbar fractures: Role of quantitative imaging. Quant Imaging Med Surg, 2016; 6(6): 772–84
8. Armitage BM, Wijdicks CA, Tarkin IS et al: Mapping of scapular fractures with three-dimensional computed tomography. J Bone Joint Surg Am, 2009; 91(9): 2222–28
9. Molenaars RJ, Mellema JJ, Doornberg JN et al: Tibial plateau fracture characteristics: Computed tomography mapping of lateral, medial, and bicondylar fractures. J Bone Joint Surg Am, 2015; 97(18): 1512–20
10. Cole PA, Mehrle RK, Bhandari M et al: The pilon map: Fracture lines and comminution zones in OTA/AO type 43C3 pilon fractures. J Orthop Trauma, 2013; 27(7): e152–56
11. Yang Y, Yi M, Zou C et al: Mapping of 238 quadrilateral plate fractures with three-dimensional computed tomography. Injury, 2018; 49(7): 1307–12
12. Xie X, Zhan Y, Dong M et al: Two- and three-dimensional CT mapping of Hoffa fractures. J Bone Joint Surg Am, 2017; 99(21): 1866–74
13. McCormack T, Karaikovic E, Gaines RW: The load sharing classification of spine fractures. Spine, 1994; 19(15): 1741–44
14. Denis F: The three column spine and its significance in the classification of acute thoracolumbar spinal injuries. Spine, 1983; 8(8): 817–31
15. Ferguson RL, Allen JB: A mechanistic classification of thoracolumbar spine fractures. Clin Orthop Relat Res, 1984; 189: 77–88
16. Dugarte AJ, Tkany L, Schroder LK et al: Comparison of 2- versus 3-dimensional fracture mapping strategies for 3-dimensional computerized tomography reconstructions of scapula neck and body fractures. J Orthop Res, 2018; 36(1): 265–71
17. Vaccaro AR, Oner C, Kepler CK et al: AOSpine thoracolumbar spine injury classification system: Fracture description, neurological status, and key modifiers. Spine, 2013; 38(23): 2028–37
18. Smith HE, Anderson DG, Vaccaro AR et al: Anatomy, biomechanics, and classification of thoracolumbar injuries. Semin Spine Surg, 2010; 22(1): 2–7
19. Stagnara P, De Mauroy JC, Dran G et al: Reciprocal angulation of vertebral bodies in a sagittal plane: Approach to references for the evaluation of kyphosis and lordosis. Spine, 1982; 7(4): 335–42
20. Lee HM, Kim HS, Kim DJ et al: Reliability of magnetic resonance imaging in detecting posterior ligament complex injury in thoracolumbar spinal fractures. Spine, 2000; 25(16): 2079–84
21. Lee JY, Vaccaro AR, Lim MR et al: Thoracolumbar injury classification and severity score: A new paradigm for the treatment of thoracolumbar spine trauma. J Orthop Sci, 2005; 10(6): 671–75
22. Vaccaro AR, Lee JY, Schweitzer KM Jr. et al: Assessment of injury to the posterior ligamentous complex in thoracolumbar spine trauma. Spine J, 2006; 6(5): 524–28
23. Ye Y, You W, Zhu W et al: The applications of finite element analysis in proximal humeral fractures. Comput Math Methods Med, 2017; 2017: 4879836

Indexed in: [Current Contents/Clinical Medicine] [SCI Expanded] [ISI Alerting System] [ISI Journals Master List] [Index Medicus/MEDLINE] [EMBASE/Excerpta Medica] [Chemical Abstracts/CAS]